

## New Insights into Cosmic Ray induced Biosignature Chemistry in Earth-like Atmospheres

MARKUS SCHEUCHER,<sup>1</sup> J. L. GRENFELL,<sup>2</sup> F. WUNDERLICH,<sup>1</sup> M. GODOLT,<sup>1</sup> F. SCHREIER,<sup>3</sup> AND H. RAUER<sup>1,2</sup>

<sup>1</sup>*Zentrum für Astronomie und Astrophysik, Technische Universität Berlin, 10623 Berlin, Germany*

<sup>2</sup>*Institut für Planetenforschung, Deutsches Zentrum für Luft- und Raumfahrt, 12489 Berlin, Germany*

<sup>3</sup>*Institut für Methodik der Fernerkundung, Deutsches Zentrum für Luft- und Raumfahrt, 82234 Oberpfaffenhofen, Germany*

(Accepted June 25, 2018)

Submitted to ApJ

### ABSTRACT

With the recent discoveries of terrestrial planets around active M-dwarfs, destruction processes masking the possible presence of life are receiving increased attention in the exoplanet community.

We investigate potential biosignatures of planets having Earth-like (N<sub>2</sub>-O<sub>2</sub>) atmospheres orbiting in the habitable zone of the M-dwarf star AD LEO. These are bombarded by high energetic particles which can create showers of secondary particles at the surface. We apply our cloud-free 1D climate-chemistry model to study the influence of key particle shower parameters and chemical efficiencies of NO<sub>x</sub> and HO<sub>x</sub> production from cosmic rays. We determine the effect of stellar radiation and cosmic rays upon atmospheric composition, temperature, and spectral appearance. Despite strong stratospheric O<sub>3</sub> destruction by cosmic rays, smog O<sub>3</sub> can significantly build up in the lower atmosphere of our modeled planet around AD LEO related to low stellar UVB. N<sub>2</sub>O abundances decrease with increasing flaring energies but a sink reaction for N<sub>2</sub>O with excited oxygen becomes weaker, stabilizing its abundance. CH<sub>4</sub> is removed mainly by Cl in the upper atmosphere for strong flaring cases and not via hydroxyl as is otherwise usually the case. Cosmic rays weaken the role of CH<sub>4</sub> in heating the middle atmosphere so that H<sub>2</sub>O absorption becomes more important. We additionally underline the importance of HNO<sub>3</sub> as a possible marker for strong stellar particle showers.

In a nutshell, uncertainty in NO<sub>x</sub> and HO<sub>x</sub> production from cosmic rays significantly influences biosignature abundances and spectral appearance.

*Keywords:* Exoplanets – Atmospheric modeling – Cosmic Rays – Biosignatures

### 1. INTRODUCTION

Cool M-dwarf stars are favored targets in exoplanetary sciences due to their high abundance in the Solar neighborhood, a close-in Habitable Zone (HZ), hence short orbital periods, and a high planet/star contrast. For an overview see e.g. [Kasting et al. \(1993\)](#); [Scalo et al. \(2007\)](#); [Shields et al. \(2016\)](#). There are however drawbacks. Planets lying in the close-in HZ could be tidally-locked (e.g. [Selsis \(2000\)](#); [Kasting et al. \(1993\)](#)) and could be bombarded by high levels of energetic particles ([Grießmeier et al. 2005](#)). An additional drawback for M-star planet habitability is the long, bright, pre-

main-sequence phase of the parent star, which may devolatilize planets that would later reside in their habitable zones (e.g. [Luger & Barnes \(2015\)](#); [Ramirez & Kaltenegger \(2014\)](#); [Tian & Ida \(2015\)](#)). Nevertheless, planets in the HZ of M-dwarf stars could represent the first opportunity to detect atmospheric properties and even biosignatures of rocky extrasolar planets. There are numerous relevant model studies e.g. in 1D ([Segura et al. 2003](#); [Segura et al. 2005](#); [Segura et al. 2010](#); [Rugheimer et al. 2015b](#); [Kopparapu et al. 2013](#); [Grenfell et al. 2012](#); [Tabataba-Vakili et al. 2016](#)) and in 3D ([Shields et al. 2013, 2016](#); [Leconte et al. 2013](#); [Yang et al. 2014](#); [Godolt et al. 2015](#); [Kopparapu et al. 2016](#)). Interpretation of such potential future observation heavily relies on our detailed understanding of atmospheric physical, chemical, and biological processes and their interaction with different electromagnetic radiation and High

Energetic Particles (HEP), such as Galactic Cosmic Rays (GCRs) and Stellar Energetic Particles (SEPs). The latter has received only limited attention in the exoplanets community so far. Our general understanding of the redistribution of incoming HEPs into secondary particles in so-called air showers through the atmosphere and their influence upon atmospheric chemistry dates back to theoretical work done in the early 1980s (Rusch et al. 1981; Solomon et al. 1981). A more recent study by Airapetian et al. (2016) investigated the production of  $N_2O$  via SEPs for the early Earth. While our own star is comparably quiescent, many M-dwarfs show high activities, in which flares with energies comparable to the devastating Carrington event on Earth in the 19th century regularly occur up to a few times a day and orders of magnitude higher energetic events have been observed, e.g. for the here studied M-dwarf AD LEO (Atri 2017; Hawley & Pettersen 1991).

Recently, potentially Earth-like planets have been found in the HZ around M-dwarfs (Proxima Cen b, LHS1140 b, and TRAPPIST-1 d-f) which may be studied in further detail with upcoming instrumentation on e.g. the James Webb Space Telescope (JWST) (Gardner et al. 2006) and E-ELT (Kasper et al. 2010). The impact of HEPs upon atmospheric chemistry needs further investigation. HEP-induced ion-pairs react with molecular oxygen, molecular nitrogen, and water to cascade into nitrogen oxides ( $NO_x = N + NO + NO_2 + NO_3$ ) and hydrogen oxides ( $HO_x = H + HO + HO_2$ ) (Porter et al. 1976; Rusch et al. 1981; Solomon et al. 1981).  $NO_x$  and  $HO_x$  catalytically destroy ozone ( $O_3$ ) in the lower and upper stratosphere respectively (Crutzen 1970) but can form  $O_3$  in the troposphere due to the so-called smog mechanism (Haagen-Smit 1952). They are stored and released from reservoir molecules such as  $HNO_3$ , depending on e.g. UV radiation and temperature. Recent model studies have shown that HEP induced  $NO_x$  and  $HO_x$  from particle showers can indeed significantly reduce  $O_3$  in an Earth-like atmosphere (Grenfell et al. 2012; Griebmeier et al. 2016; Tabataba-Vakili et al. 2016). Production rates of around 1.27  $NO_x$  (Porter et al. 1976; Rusch et al. 1981) and 2.0  $HO_x$  (Solomon et al. 1981) per ion pair have been assumed in numerous atmospheric studies, but recent ion-chemistry studies by e.g. Sinnhuber et al. (2012) and Verronen & Lehmann (2013) have pointed out that the uncertainties in these complex chemical coupling coefficients might be under-estimated, especially when additionally taking into account negative ion chemistry. When conducting numerical studies of rocky planets around active M-dwarfs, such uncertainties can have a major impact on atmospheric abundances - including species influenced by biogenic processes.  $O_3$ , for exam-

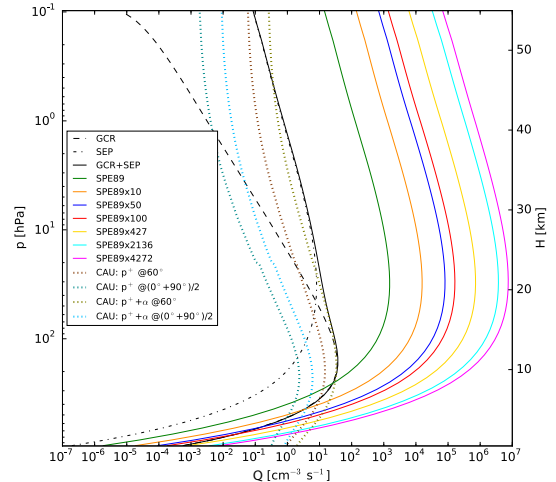


**Figure 1.** Ion pair production rate ( $Q$ ) profiles for different HEP fluxes through Earth's atmosphere calculated in our model (solid). Co-plotted are comparison profiles with PLANETOCOSMICS (CAU) (dotted) for protons ( $p^+$ ) and alpha particles ( $\alpha$ ) and different locations on Earth ( $60^\circ$  latitude, or the average of polar ( $90^\circ$ ) and equatorial ( $0^\circ$ )). Black lines represent solar minimum conditions on Earth from our model, with air showers from GCRs (dashed), SEPs (dash-dotted), and both combined (solid). The other solid lines represent  $Q$ -profiles for a theoretical flaring Sun, shown in multiples of the SPE89 (green), where fluxes in all energy ranges were multiplied by 10 (orange), 50 (blue), and 100 (red).  $Q$ -profiles SPE89x427 (yellow), SPE89x2136 (cyan), and SPE89x4272 (magenta), represent separate cases where Earth at 1 AU would receive the same SEP flux density as a virtual Earth around AD LEO at a distance of 0.153 AU with stellar flaring strengths of SPE89x10 (orange), SPE89x50 (blue), and SPE89x100 (red), respectively.

ple is removed catalytically by  $HO_x$  and  $NO_x$ . Also,  $CH_4$  is usually removed by  $OH$ , a member of the  $HO_x$  family.

Based on the above, the main motivation of this work is to compare the influence of different M-dwarf stellar flaring energies to that of the uncertainties in atmospheric  $NO_x$ - $HO_x$  production efficiencies from incoming SEPs and show their impact on overall climate and spectral features in transit observations. In Section 2 we describe the models used for this work and motivate the modeled scenarios, in Section 3 we briefly describe our results, before discussing and comparing them to other relevant works in Section 4. Finally, in Section 5 we draw our conclusions.

## 2. MODELING FRAMEWORK

### 2.1. Model description

We investigate the influence of GCRs and SEPs from quiescent and flaring stars, on atmospheric chemistry and potential biosignatures like  $O_3$ , nitrous oxide ( $N_2O$ ),

**Table 1.** Model scenarios in this work. ‘Star’ indicates here the host star of our planet, ‘distance’ shows the orbital distance of our planet to its host star, and ‘HEP’ is the energetic particle bombardment on our planet.  $f_{\text{NOX}}$  and  $f_{\text{HOX}}$  are the chemical air shower production efficiencies for NOX and HOX production per ion pair respectively, studied for each configuration.

Star	Distance [AU]	HEPs	$f_{\text{NOX}}$	$f_{\text{HOX}}$
Sun	1.0	GCR		
		SEP		
		SPE89	1.0	0.0
		SPE89x10	1.27	1.0
		SPE89x50	1.44	2.0
		SPE89x100	1.6	
		SPE89x427	2.0	
		SPE89x2136		
AD LEO	0.153	GCR	1.0	0.0
		SEP	1.27	1.0
		SPE89	1.44	2.0
		SPE89x10	1.6	
	0.161	SPE89x50	2.0	
		SPE89x100		

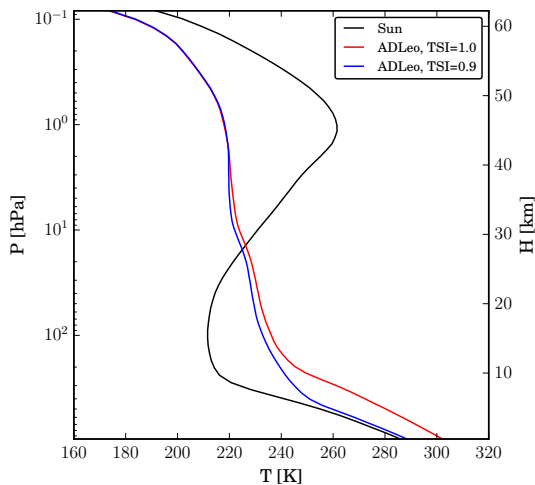


**Figure 2.** Temperature profiles for Earth around Sun (black), Earth around AD LEO at a distance of 0.153 AU where  $\text{TSI} = 1.0 \text{ TSI}_{\oplus}$  (red), and Earth around AD LEO at 0.161 AU or  $0.9 \text{ TSI}_{\oplus}$  (blue), all with GCR background.

$\text{CH}_4$ , and chloromethane ( $\text{CH}_3\text{Cl}$ ). We build upon our stationary, global mean, cloud-free coupled climate-chemistry 1D model (Tabataba-Vakili et al. 2016), and update the cosmic rays’ propagation. First we compute the fluxes of primary HEPs, either GCRs or SEPs, that arrive at the top of our model atmosphere (TOA) at 6.6

Pa, using the magnetospheric model from Griebmeier et al. (2005, 2009). For Earth reference cases we take GCR and SEP measurements outside the Earth’s magnetic field for solar minimum conditions and use cut-off energies from Griebmeier et al. (2016) for Earth’s magnetic shielding. For exoplanet runs we assume the same planetary magnetic field, but scale the HEP fluxes in all energy ranges as follows. For SEPs we use a simplified (conservative) inverse squared scaling with distance from the star (see Grenfell et al. (2012)), hence neglect possible magnetic diffusion processes in the heliosphere, which would further increase the power-law exponent beyond 2.0 in the scaling of HEP fluxes for short-period orbits. We partly compensate for this effect with higher intrinsic HEP flux scenarios from the star (see Model scenarios). For GCRs at exoplanets we adopt enhanced shielding modulation closer to the star, as described by Griebmeier et al. (2009). Once we have the TOA HEP fluxes, we use the Gaisser-Hillas approach (see e.g. Tabataba-Vakili et al. (2016)) to calculate the atmospheric ion pair production profiles ( $Q$ ). In the case of Earth, we can compare our approach to more sophisticated models like e.g. the PLANETOCOSMICS Monte Carlo simulations of the cosmic ray induced secondary-particle showers performed by the Christian-Albrechts University (CAU) in Kiel, Germany (Fichtner et al. 2013), and find them to be in qualitatively good agreement, as shown in Fig. 1. Consequently, these ion pairs cascade into NOX and HOX species. The NOX-HOX production efficiencies describing how many NOX and HOX are subsequently produced per cosmic rays induced ion pair are widely used in ion chemistry models with values that were calculated by Rusch et al. (1981) and Solomon et al. (1981). These values are based on an Earth atmospheric composition assuming ionization to be directly proportional to ionization cross sections, which themselves are taken to be independent of pressure and temperature. Note that negative ion chemistry was taken into account much later by Verronen & Lehmann (2013) which further influences the NOX-HOX production efficiencies. In our study we made the cosmic rays air-shower parameters in our climate-chemistry model flexible so we can analyze the influence of the uncertainties of these chemical production efficiencies  $f_{\text{NOX}}$  and  $f_{\text{HOX}}$  on potential biosignatures compared to the impact of potential stellar flaring scenarios.

Lastly, transit spectra i.e. transmission spectra ( $\mathcal{T}(\lambda)$ ) are calculated using the ‘Generic Atmospheric Radiation Line-by-line Infrared Code’ GARLIC (Schreier et al. 2014) that has been extensively verified (e.g. Schreier et al. 2018a) and validated (Schreier et al.

2018b), a FORTRAN90 version of MIRART/SQUIRRL (see e.g. von Clarmann et al. (2003); Melsheimer et al. (2005)) used by (e.g. Rauer et al. 2011; Griebmeier et al. 2016; Tabataba-Vakili et al. 2016). In this study we use GARLIC with HITRAN2012 (Rothman et al. 2013) along with the ‘CKD’ continua (Clough, Kneizys, & Davies 1989) for calculations of line absorption and Rayleigh scattering parameterization from Sneep & Ubachs (2005); Marcq et al. (2011); Murphy (1977). We use temperature, pressure, water vapor, and concentration profiles of those species (23 in total<sup>1</sup>) which are present in both HITRAN2012 as well as in our climate-chemistry model. The corresponding transit depths  $\delta(\lambda)$  are calculated using:

$$\delta(\lambda) = \left( \frac{r_p + h(\lambda)}{r_s} \right)^2, \quad (1)$$

where  $r_p$  is the planetary radius,  $r_s$  the stellar radius, and  $h(\lambda) = \sum_i (1 - \tau_i(\lambda)) \Delta h_i$  is the effective height of the atmosphere for a given wavelength.

## 2.2. Model scenarios

In this study we lay focus on virtual Earth-like planets around the active red M4.5 dwarf star AD Leonis, hereafter AD LEO. In doing so, we place a virtual Earth (1g planet, 1 atm. surface pressure, albedo of 0.21 - tuned to obtain global mean surface temperatures of 288.15 K on Earth) in the HZ around AD LEO in two different positions, starting with the Earth US standard 1976 reference atmosphere (COESA) and allow the climate and chemistry to relax into a new steady state solution. First we start with an Earth around the Sun reference case, using the incoming stellar electromagnetic flux based on Gueymard (2004). To be comparable with earlier studies we next place the planet at a distance of 0.153 AU around AD LEO, where the Total Stellar Irradiance (TSI) equals the amount the Earth receives from the Sun, before moving it further outwards to 0.161 AU (0.9  $\text{TSI}_{\oplus}$ ) around AD LEO where it receives only 90% of Earth’s TSI. In all AD LEO cases we use the electromagnetic spectrum based on Segura et al. (2005). The former approach of 1.0  $\text{TSI}_{\oplus}$  together with an Earth-like relative humidity profile (Manabe & Wetherald 1967) leads to surface temperatures larger than 288K (see also scaling arguments in Segura et al. (2003) and references therein). Various modeling studies, including early 1D

studies (e.g. Cess 1976; Kasting & Ackerman 1986), as well as more recent 3D studies (e.g. Leconte et al. 2013; Popp et al. 2015; Godolt et al. 2016; Fujii et al. 2017) have argued that for increased surface temperatures the relative humidity profile may differ from that of the Earth (eg. Manabe & Wetherald 1967), which we use here and has also been assumed in previous studies (Segura et al. 2010; Rauer et al. 2011; Grenfell et al. 2012; Rugheimer et al. 2015a). Other studies, e.g. Kasting et al. (1993) and Kopparapu et al. (2013), assume a fully saturated atmosphere and find that an Earth-like planet around AD Leo would be close to or even inside the inner edge of the habitable zone. This assumption of a fully saturated atmosphere may however overestimate the water concentrations, as shown by 3D studies, see e.g. Leconte et al. (2013); Yang et al. (2014); Kopparapu et al. (2016). 3D modeling results by Shields et al. (2013) show that an Earth-like planet around AD LEO receiving 90% insolation may have similar surface temperatures as the Earth around the Sun. Hence, for this case, the assumption of an Earth-like relative humidity profile to determine the water profile in the 1D model seems to be better justified and in line with 3D model results (see e.g. Godolt et al. (2016)). Whereas the approach of placing the planet at 0.161 AU (0.9  $\text{TSI}_{\oplus}$ ) around AD LEO is model dependent, it has the advantage of lying closer to Earth conditions, where our model is validated.

For each of the above cases we investigate various stellar activity scenarios for the HEP shower through the atmosphere, all based on measurements on Earth, and scaled for AD LEO according to the above mentioned functions. We start with GCR and SEP stellar-minimum background cases, as described above. Then we compare various stellar flaring scenarios, all based on GOES 6 and 7 measurements of the medium-hard spectrum flare that hit the Earth in 1989 (Smart & Shea 2002), hereafter SPE89. We assume quasi-constant flaring conditions i.e. a flaring frequency faster than the relevant chemical response timescales to investigate long term climate and composition effects of such violent environments rather than short-term variations. We justify our assumption since e.g. Earth’s mean  $\text{O}_3$  column does not change significantly with the day-night cycle whereas flaring on AD LEO has been extensively measured to be in the order of a few per day, with event energies exceeding those of the largest recorded events on Earth ( $\sim 10^{32}$ erg) (Atri 2017). Additionally, from the KEPLER survey we have multiple M-star observations with flaring energies of up to  $10^{36}$ erg and frequencies of up to 100 times those of G-stars (Maehara et al. 2012; Shibayama et al. 2013; Candelaresi et al. 2014). With this in mind, we model

<sup>1</sup> Atmospheric species used for transmission spectra in GARLIC are: OH,  $\text{HO}_2$ ,  $\text{H}_2\text{O}_2$ ,  $\text{H}_2\text{CO}$ ,  $\text{H}_2\text{O}$ ,  $\text{H}_2$ ,  $\text{O}_3$ ,  $\text{CH}_4$ ,  $\text{CO}$ ,  $\text{N}_2\text{O}$ ,  $\text{NO}$ ,  $\text{NO}_2$ ,  $\text{HNO}_3$ ,  $\text{ClO}$ ,  $\text{CH}_3\text{Cl}$ ,  $\text{HOCl}$ ,  $\text{HCl}$ ,  $\text{ClONO}_2$ ,  $\text{H}_2\text{S}$ ,  $\text{SO}_2$ ,  $\text{O}_2$ ,  $\text{CO}_2$ ,  $\text{N}_2$

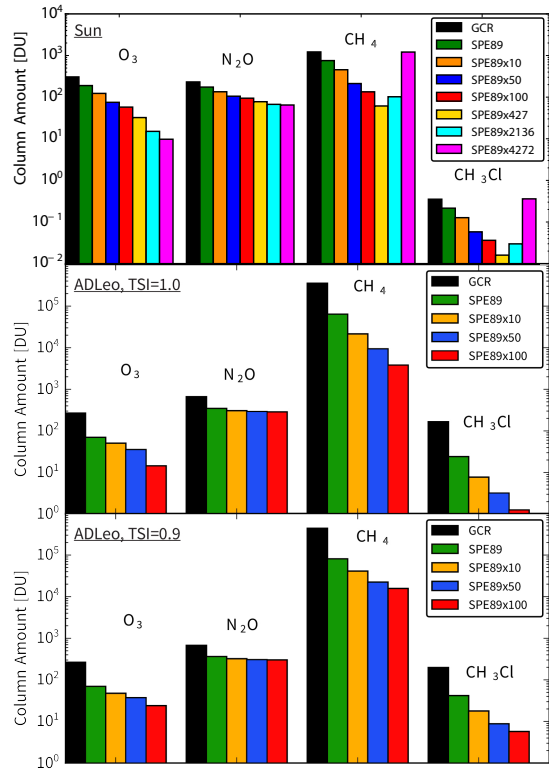
higher flaring scenarios by multiplying the SPE89 particle fluxes in all energy ranges by 10, 50, and 100. For AD LEO runs this adds to the ( $\sim 40x$ ) enhanced flux density due to proximity to the host star. This means that our virtual Earth at a distance of 0.153AU around an AD LEO flaring with 100 times enhanced SPE89 strength, hereafter SPE89x100, actually receives 4272 times the SEP flux than Earth received during SPE89. For comparison we also investigated an Earth in its current position receiving the same SEP flux densities and added these three scenarios as separate cases only for Earth around the Sun cases, flaring with SPE89x427, SPE89x2136, and SPE89x4272 to compare to the AD LEO SPE89x10, SPE89x50, and SPE89x100 cases, respectively.

Lastly, for all of the above scenarios, we perform our parameter study and vary the NO<sub>x</sub>-HO<sub>x</sub> production efficiencies per cosmic rays induced ion pair ( $Q$ ) within their plausible parameter ranges (Rusch et al. 1981; Solomon et al. 1981; Sinnhuber et al. 2012; Verronen & Lehmann 2013) for every combination of  $f_{\text{NO}_x} = [1.0, 1.27, 1.44, 1.6, 2.0]$  and  $f_{\text{HO}_x} = [0.0, 1.0, 2.0]$ . The full set of model scenarios can be seen in Table 1.

We would like to remark that in the thought experiment of an Earth-like planet around AD LEO we assume that life would still be present in the form of biogenic surface emissions as on Earth even in the highest flaring cases, despite the hostility from its host star. Also we assume Earth’s evolutionary history, and a mean global daytime-average, which might not strictly hold in the case of tidal-locking. We do this for the sake of simplicity to study the impact of HEPs alone.

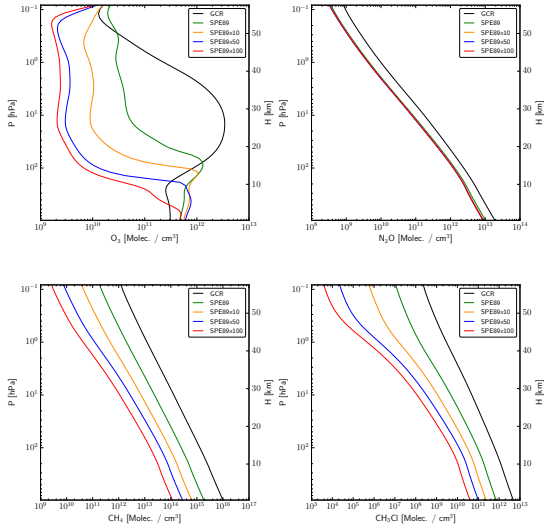
### 3. RESULTS

Figure 2 shows the atmospheric temperature profiles for our three planetary positions, Earth around Sun (black), virtual Earth around AD LEO at a distance of 0.153 AU with a  $\text{TSI} = 1.0 \text{ TSI}_{\oplus}$  (red), and virtual Earth around AD LEO at 0.161 AU with a  $\text{TSI} = 0.9 \text{ TSI}_{\oplus}$  (blue), all with scaled GCR background. The reference is always the GCR background, but solar minimum SEP background leads to indistinguishable results for our analysis and is therefore not shown in this work. Until stated otherwise, we show results for the chemical air shower production efficiencies  $f_{\text{NO}_x} = 1.27$  and  $f_{\text{HO}_x} = 2.0$ , in order to be comparable to other works. For the M-dwarf case at  $1.0 \text{ TSI}_{\oplus}$  (red), we calculate an increase in surface temperature to over 300 K mainly due to an enhanced methane greenhouse as found in previous works (e.g. Segura et al. (2005)). In addition the stratospheric temperature inversion is essentially non-existent mainly because of the lower



**Figure 3.** Atmospheric column amounts for O<sub>3</sub>, N<sub>2</sub>O, CH<sub>4</sub>, and CH<sub>3</sub>Cl, presented in Dobson units ( $1 \text{ DU} = 2.687 \times 10^{16} \text{ molec./cm}^2$ ) for Earth around Sun (top), Earth around AD LEO at  $\text{TSI} = 1.0 \text{ TSI}_{\oplus}$  (middle), and Earth around AD LEO at  $0.9 \text{ TSI}_{\oplus}$  (bottom). In each panel we show model runs for GCR background (black), stellar flaring scaled from the SPE89 on Earth (green), and the enhanced flaring runs SPE89 multiplied by 10 (orange), 50 (blue), and 100 (red). All particle fluxes received by the planet are scaled from the observed value (@ 1AU) to the appropriate planetary orbital distance. Results for solar minimum SEP background are indistinguishable from GCR background, and therefore not shown. The upper panel additionally shows the three cases (SPE89x427 (yellow), SPE89x2136 (cyan), and SPE89x4272 (magenta)) where the Earth around Sun would receive the same SEP flux density from the Sun as the virtual Earth around AD LEO at  $\text{TSI}=1.0 \text{ TSI}_{\oplus}$  (middle panel) receives from an AD LEO flaring with SPE89x10 (orange), SPE89x50 (blue), and SPE89x100 (red) strength, respectively (see Sec. 2 for further explanation).

near-UV flux compared to the Sun, which reduces O<sub>3</sub> abundance and heating, as already discussed in previous studies (Segura et al. 2010; Rauer et al. 2011). On moving the planet further away from AD LEO to 0.161 AU ( $0.9 \text{ TSI}_{\oplus}$ ), the surface temperature in our model reaches Earth-like 289 K, similar to the results of Shields et al. (2013), also lacking the stratospheric temperature inversion. The position of the tropopause (i.e. end of convective regime) in these two AD LEO runs changes significantly from 11 km for the  $1.0 \text{ TSI}_{\oplus}$  case to 5.5



**Figure 4.** Molecular profiles for our virtual Earth around AD LEO at 1.0  $\text{TSI}_{\oplus}$  as in Fig. 3 (middle panel) and red line in Fig. 2. The ozone profile (upper left),  $\text{N}_2\text{O}$  (upper right), methane (lower left), and  $\text{CH}_3\text{Cl}$  profile (lower right) are each compared for the different flaring scenarios from Fig. 3 (middle).

km for the 0.9  $\text{TSI}_{\oplus}$  case, compared to  $\sim 8.5$  km for our Earth around Sun case.

Figure 3 shows atmospheric column amounts of  $\text{O}_3$ ,  $\text{N}_2\text{O}$ ,  $\text{CH}_4$ , and  $\text{CH}_3\text{Cl}$ , in Dobson units ( $1 \text{ DU} = 2.687 \times 10^{16} \text{ molec./cm}^2$ ) for the same planet-star configurations as in Fig. 2. For each configuration we compare runs with different HEP conditions and show the GCR background run (black) as reference. We compare different stellar flaring strengths by multiplying the measured fluxes from SPE89 and scaling the incoming particle flux to the planet’s position for the AD LEO runs. The different flaring strength cases vary from SPE89x1 to SPE89x100 for AD LEO runs and from SPE89x1 to SPE89x4272 for Earth around Sun runs (see Fig. 3). As expected, with increasing flaring strength the  $\text{O}_3$  column is depleted, similar to results of e.g. Grenfell et al. (2012) and Tabataba-Vakili et al. (2016). The same holds qualitatively for  $\text{N}_2\text{O}$  although note that we calculate here a ‘saturation’ behavior i.e. where increasing flaring energy has no further effect upon the  $\text{N}_2\text{O}$  column. Both the  $\text{CH}_4$  and  $\text{CH}_3\text{Cl}$  columns also follow the same trend of depletion e.g. from  $\sim 1.6$  ppmv Earth tropospheric  $\text{CH}_4$  concentrations down to  $\sim 0.2$  ppmv of tropospheric  $\text{CH}_4$  in the SPE89x100 case. An exception presents the interesting increase in  $\text{CH}_4$  and  $\text{CH}_3\text{Cl}$  for our most active Sun cases (upper panel), SPE89x2136 (cyan), and SPE89x4272 (magenta), which were added for comparison purposes with the AD LEO cases and which we will discuss in Section 4. When we compare

the GCR background runs for Earth around Sun with AD LEO, we see an increase of two orders of magnitude in the  $\text{CH}_4$  and  $\text{CH}_3\text{Cl}$  column amounts around AD LEO due to slower  $\text{O}_3$  photolysis resulting in lower OH densities, as discussed in Segura et al. (2005).

In order to investigate the column behavior in Fig. 3, Fig. 4 shows the atmospheric profiles in molecules/ $\text{cm}^3$  in the case of our virtual Earth around AD LEO at 1.0  $\text{TSI}_{\oplus}$  as in Fig. 3 (middle panel). The color coding for different flaring strengths is the same as in Fig. 3. We calculate stratospheric ozone loss (upper left) with increasing influx of SEPs, compared to a quiescent AD LEO (black), as well as increased ozone in the troposphere, which is discussed in Section 4. The  $\text{N}_2\text{O}$  (upper right) on the other hand, responds only weakly to increasing flare strength, decreasing from  $\sim 800$  ppbv ( $2 \times 10^{13} \text{ Molec./cm}^3$ ) (GCR case) to  $\sim 250$  ppbv ( $9 \times 10^{12} \text{ Molec./cm}^3$ ) (SPE89x100) in the lower atmosphere. Methane and  $\text{CH}_3\text{Cl}$  (lower row) both feature lower concentrations throughout the whole atmosphere with increasing flare strength. The greatly enhanced surface concentration of  $\sim 400$  ppmv ( $10^{16} \text{ Molec./cm}^3$ )  $\text{CH}_4$  and  $\sim 200$  ppbv ( $5 \times 10^{12} \text{ Molec./cm}^3$ )  $\text{CH}_3\text{Cl}$  in the AD LEO GCR case (compared to  $\sim 1.6$  ppmv ( $3.9 \times 10^{13} \text{ Molec./cm}^3$ )  $\text{CH}_4$  and  $\sim 0.5$  ppbv ( $1.2 \times 10^{10} \text{ Molec./cm}^3$ )  $\text{CH}_3\text{Cl}$  Earth tropospheric concentrations) decreases in our simulations down to  $\sim 5$  ppmv ( $10^{14} \text{ Molec./cm}^3$ ) of  $\text{CH}_4$  and  $\sim 2$  ppbv ( $4 \times 10^{10} \text{ Molec./cm}^3$ )  $\text{CH}_3\text{Cl}$  for the AD LEO SPE89x100 case.

In order to investigate the methane response, whose main sinks are OH (lower to mid atmosphere) and Cl (upper atmosphere), we analyze chlorine containing species in our model atmospheres in Fig. 5. For all our three planetary configurations we compare background GCR runs (black) with the 50 times enhanced SPE89 flaring cases (blue). The solid lines represent total chlorine ( $\text{Cl}_y$ ) i.e. the sum of all chlorine-bearing species, which increases by two orders of magnitude in molecules/ $\text{cm}^3$  when we go from the Earth to an Earth-like planet around AD LEO. For all cases the majority of stratospheric chlorine is in the form of HCl (dashed), while in the upper stratosphere, atomic chlorine, Cl, also reaches significant levels above 40 km. This is the region where  $\text{CH}_4$  production becomes controlled by Cl (dash-dotted), instead of OH, which is the major methane destroying reaction below around 40 km, as discussed in Section 4.  $\text{ClONO}_2$  (dotted) is only the dominant chlorine-bearing species for a small fraction in Earth’s mid-stratosphere for quiescent solar cases.

Fig. 6 compares the influence of varying the chemical air shower production efficiencies  $f_{\text{NOX}}$  and  $f_{\text{HOX}}$  for the different flaring cases for the Earth (top), the 1.0  $\text{TSI}_{\oplus}$

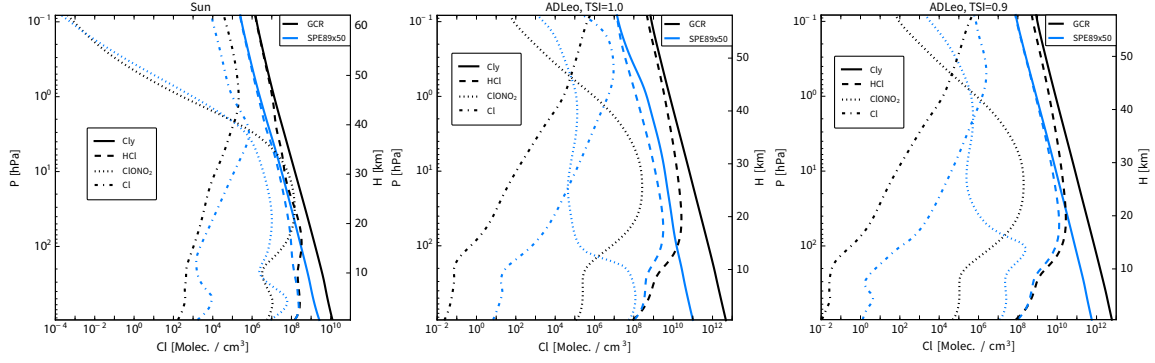


**Figure 5.** Atmospheric profiles of several species containing chlorine for the Earth around Sun case (left), AD LEO at 1.0  $\text{TSI}_{\oplus}$  (middle), and AD LEO at 0.9  $\text{TSI}_{\oplus}$  (right). For each case we compare runs with GCR background (black) with runs for 50 times enhanced SPE89 flaring cases (blue). We show the sum of all chlorine containing species (Cly) in our model (solid), HCl (dashed),  $\text{ClONO}_2$  (dotted), and atomic Cl (dash-dotted).

AD LEO case (middle), and the 0.9  $\text{TSI}_{\oplus}$  AD LEO case (bottom). We show the resulting ozone profiles (left), temperature (middle), and the UVB environment profile in  $\text{W}/\text{m}^2$  (right). Shades of green represent the SPE89 flaring cases for different SEP induced NOX-HOX production efficiencies; shades of orange represent the same runs for 10 times enhanced flaring and shades of blue represent the 100 times enhanced flaring cases respectively. Within the green, orange, and blue scenarios, darkest colors represent the lowest parameter values  $f_{\text{NOX}}=1.0$  and  $f_{\text{HOX}}=0.0$ , while lightest colors represent the highest values of  $f_{\text{NOX}}=2.0$  and  $f_{\text{HOX}}=2.0$ , with all other combinations in between. For all quiescent star (GCR) cases (black) all modeled combinations of  $f_{\text{NOX}}$  and  $f_{\text{HOX}}$  result in virtually indistinguishable profiles, hence only the cases of  $f_{\text{NOX}}=1.27$  NOX/Q, and  $f_{\text{HOX}}=2.0$  HOX/Q, as used by other works, are shown. For the Earth around Sun case, results suggest that the influence of changing the NOX-HOX production efficiencies is less important than varying the Sun’s flaring strength i.e. amount of incoming SEPs. In the AD LEO cases on the other hand,  $f_{\text{NOX}}$  and  $f_{\text{HOX}}$  influence at least the atmospheric temperature and ozone profiles significantly, up to a point where for the 0.9  $\text{TSI}_{\oplus}$  case, a high flaring AD LEO (50 times enhanced SPE89) can lead to an atmospheric temperature profile similar to a quiescent AD LEO case, if the chemical air shower parameters through the planet’s atmosphere are  $f_{\text{NOX}}=2.0$  and  $f_{\text{HOX}}=0.0$ . In contrast with  $f_{\text{NOX}}=2.0$  and  $f_{\text{HOX}}=2.0$ , the temperature may be reduced by up to 40 K throughout almost the whole stratosphere. To investigate whether the above mentioned differences in stratospheric temperature and composition due to different NOX-HOX production efficiencies in the SPE89x50 strong flaring AD LEO cases with a planet at 0.9  $\text{TSI}_{\oplus}$  (bottom row of Fig. 6) have any distinguishable effect on atmospheric spectra, Fig. 7 shows the cor-

responding transit depths  $\delta(\lambda)$ . The spectra are shown with constant spectral resolution  $R = \lambda/\Delta\lambda = 100$  over the wavelength range from 0.3-30  $\mu\text{m}$ . This corresponds to e.g. one mode of the near infrared spectrograph NIR-Spec onboard the upcoming JWST mission. We show the contribution of the planetary body i.e. without the atmospheric contribution (dashed-black), which we calculate to be 551.3 ppm. Similar to before, our reference case is the GCR background (black) with  $f_{\text{NOX}}=1.27$  and  $f_{\text{HOX}}=2.0$ , because runs for all above described combinations of  $f_{\text{NOX}}$  and  $f_{\text{HOX}}$  for GCR or SEP background cosmic rays result in qualitatively identical atmospheric concentration profiles for all our modeled molecules. First, we compare this to the SPE89x50 run for  $f_{\text{NOX}}=2.0$  and  $f_{\text{HOX}}=0.0$  (dashed-blue) that results in an almost indistinguishable stratospheric temperature profile. We see the destruction of ozone due to flaring in the weakened 9.6  $\mu\text{m}$  absorption band as well as reduced absorption by water and methane in the near-infrared (1-2  $\mu\text{m}$ ). We also see  $\text{HNO}_3$  absorption above 10 microns becoming visible. The second comparison in Fig. 7 is with the SPE89x50 run for  $f_{\text{NOX}}=2.0$  and  $f_{\text{HOX}}=2.0$  (light blue). Here we see even stronger suppression of the near-infrared water and methane features, and even stronger  $\text{HNO}_3$  absorption in the far-infrared. There are also new  $\text{HNO}_3$  features visible around 17 and 21  $\mu\text{m}$ . The 9.6  $\mu\text{m}$   $\text{O}_3$  absorption band is a little less reduced than in the  $f_{\text{HOX}} = 0.0$  case, due to NOX-HOX reactions, that limit the NOX sink for  $\text{O}_3$ , similar to Tabataba-Vakili et al. (2016). All three runs clearly show the slope due to Rayleigh scattering towards the visible and into the ultraviolet.

To further explain the differences in the transit spectra of Fig. 7, Fig. 8 shows the corresponding atmospheric profiles of temperature,  $\text{O}_3$ ,  $\text{CH}_4$ ,  $\text{H}_2\text{O}$ ,  $\text{N}_2\text{O}$ , and  $\text{HNO}_3$  for the three AD LEO runs at 0.9  $\text{TSI}_{\oplus}$  using the same color scheme ( $\text{O}_3$  and temperature are also

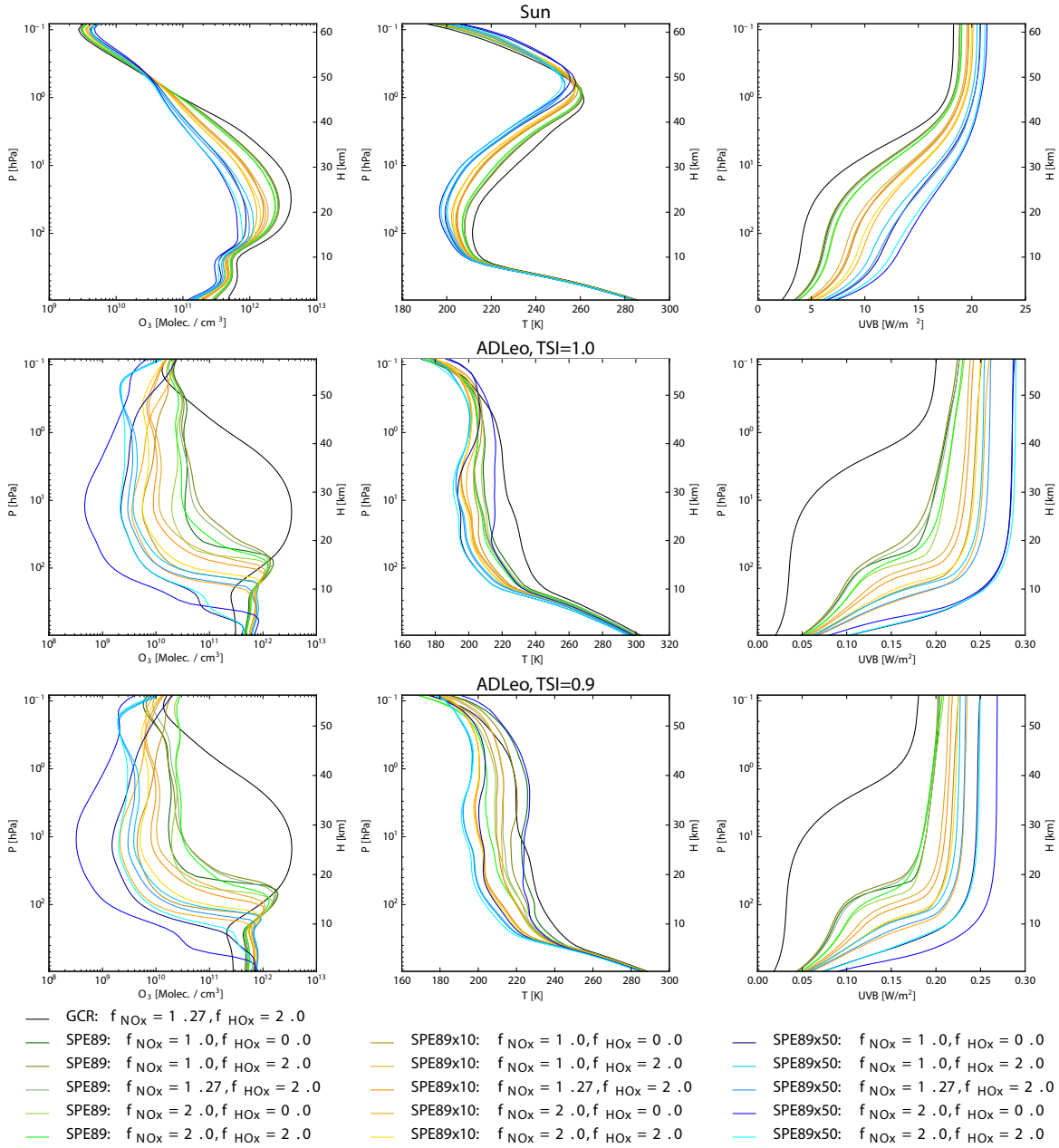


**Figure 6.** The influence of chemical NO<sub>x</sub>-HO<sub>x</sub> fractionation of HEP-induced ion pairs for the flaring scenarios from Fig. 3, except the highest flaring cases SPE89x100. The rows show cases for Earth around Sun (top three panels), Earth around AD LEO at 1.0 TSI<sub>⊕</sub> (middle three panels), and Earth around AD LEO at 0.9 TSI<sub>⊕</sub> (bottom three panels). Columns show O<sub>3</sub> (left), temperature (middle), and UVB (right). The color ranges represent the GCR reference case (black), SPE89 (green colors), SPE89 x 10 (orange colors), and SPE89 x 50 (blue colors). The different shades of green, orange, and blue, represent model runs with different NO<sub>x</sub>-HO<sub>x</sub> fractionation for the same respective HEP case.

shown and explained in Fig. 6). Compared to the GCR case (black) with a fairly constant CH<sub>4</sub> concentration of ~500 ppmv ( $1.3 \times 10^{16}$  Molec./cm<sup>3</sup>) throughout our model atmosphere CH<sub>4</sub> is reduced throughout the whole atmosphere in both SPE89x50 cases,  $f_{\text{NO}_x}=2.0$  and  $f_{\text{HO}_x}=0.0$  (dashed-blue) resulting in ~60 ppmv ( $1.4 \times 10^{15}$  Molec./cm<sup>3</sup>) CH<sub>4</sub>, and  $f_{\text{NO}_x}=2.0$  and  $f_{\text{HO}_x}=2.0$  (light blue) leaving ~20 ppmv ( $5 \times 10^{14}$

Molec./cm<sup>3</sup>) CH<sub>4</sub>. The H<sub>2</sub>O profiles show similar behavior, although the H<sub>2</sub>O abundance is clearly less affected by the HEPs in the SPE89x50  $f_{\text{HO}_x}=0.0$  case, with still ~60-100 ppmv ( $\sim 10^{14}$  Molec./cm<sup>3</sup>) in the mid and upper atmosphere than in the SPE89x50  $f_{\text{HO}_x}=2.0$  case leaving only ~2-20 ppmv ( $\sim 2 \times 10^{12}$  Molec./cm<sup>3</sup>) in the mid and upper atmosphere, similar to the according temperature profiles. Again, N<sub>2</sub>O

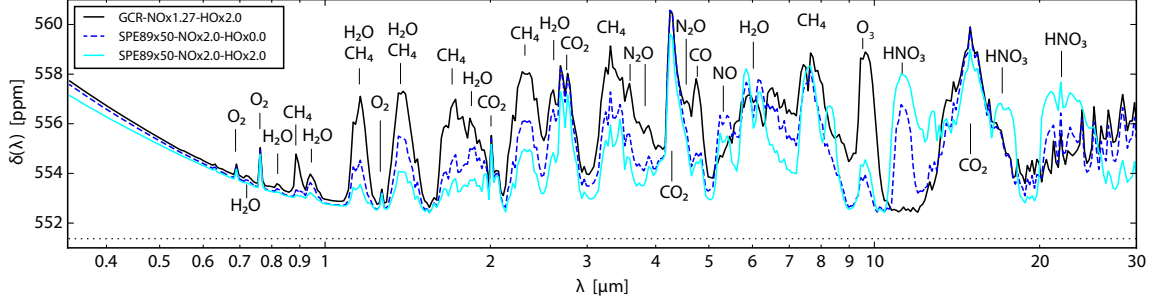


**Figure 7.** Modeled transit depths  $\delta(\lambda)$  in parts per million over wavelength  $\lambda$  ( $R=100$ ) for a virtual Earth around AD LEO at  $0.9 \text{ TSI}_{\oplus}$ . Shown are three runs from the bottom row of Fig. 6: GCR (black), and the last two runs of the high flaring case SPE89x50: one with  $f_{\text{NOX}} = 2.0$  and  $f_{\text{HOX}} = 0.0$  (dashed-blue) that shows a similar temperature profile to the GCR case, and one with  $f_{\text{NOX}} = 2.0$  and  $f_{\text{HOX}} = 2.0$  (light-blue) that shows significantly reduced stratospheric temperatures. The dotted black line at the bottom represents the transit depth for the virtual planet without atmosphere (551.3 ppm).

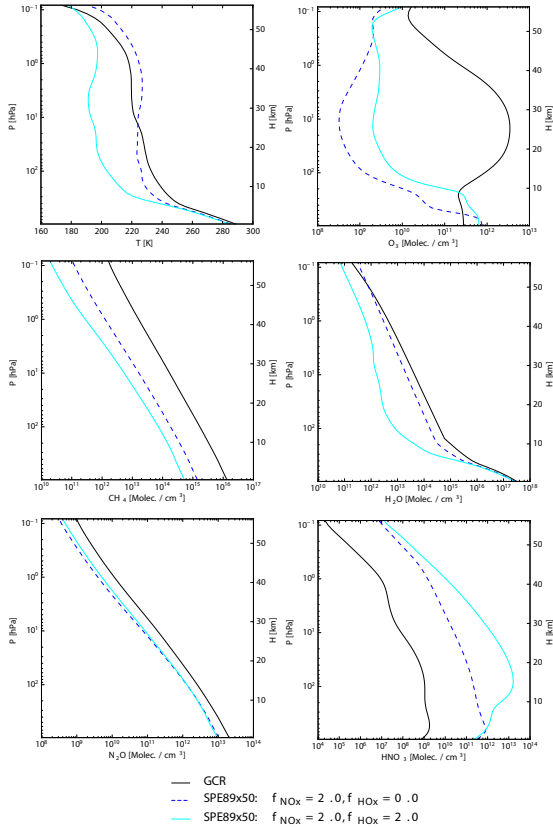


**Figure 8.** Atmospheric Profiles of temperature,  $\text{O}_3$ ,  $\text{CH}_4$ ,  $\text{H}_2\text{O}$ ,  $\text{N}_2\text{O}$ , and  $\text{HNO}_3$  for a virtual Earth around AD LEO at  $0.9 \text{ TSI}_{\oplus}$ . Shown are the three runs analyzed in Fig. 7: GCR (black), and the last two runs of the high flaring case SPE89x50:  $f_{\text{NOX}} = 2.0$  and  $f_{\text{HOX}} = 0.0$  (dashed-blue) and  $f_{\text{NOX}} = 2.0$  and  $f_{\text{HOX}} = 2.0$  (light-blue).

shows only weak responses to both, flaring, and  $f_{\text{HOX}}$  variation. The  $\text{HNO}_3$  profiles in both SPE89x50 cases are greatly enhanced, as seen in the spectra in Fig. 7. In the lower and mid stratosphere  $\text{HNO}_3$  is further increased in the  $f_{\text{HOX}}=2.0$  case peaking at  $\sim 8$  ppmv

( $2 \times 10^{13} \text{ Molec./cm}^3$ ), which is about ten thousand times the modern Earth's atmospheric concentration, compared to the  $f_{\text{HOX}}=0.0$  case resulting in only  $\sim 90$  ppbv ( $\sim 3\text{-}5 \times 10^{11} \text{ Molec./cm}^3$ )  $\text{HNO}_3$ , which explains the additional spectral  $\text{HNO}_3$  features in Fig. 7.

#### 4. DISCUSSION

In this study we analyze how increased HEP fluxes associated with active M-stars like AD LEO, influence the atmospheric chemistry and climate of Earth-like planets in comparison to the impact of chemical production efficiencies. Our special focus lies on biosignatures i.e. species which on Earth are associated with life. Our results in Fig. 2 (red line) show that the surface temperature would increase by over 12 K on placing a virtual Earth-like planet at  $1.0 \text{ TSI}_{\oplus}$  around AD LEO when assuming an Earth-like relative humidity profile. However, such a temperature increase would likely change the hydrological cycle leading to a strong water feedback, as shown for a planet around K-stars by Godolt et al. (2015). This could place such planets outside the HZ as suggested by e.g. Kopparapu et al. (2013). Assuming a planet around AD LEO that receives only 90%  $\text{TSI}_{\oplus}$  (blue line), we obtain a moderate surface temperature of 289 K, which is in good agreement with the 3D model results of Shields et al. (2013).

Results for different flaring strengths of the same star (Fig. 3) suggest stratospheric  $\text{O}_3$  destruction with increasing HEP fluxes due to increased catalytic destruction from mainly NOX. All our runs for Sun and AD LEO show this trend. As indicated in Fig. 6, the effect of increasing flaring energy upon  $\text{O}_3$  is different for Earth, compared with an Earth-like planet around AD LEO. While Earth would moderately lose  $\text{O}_3$  in the troposphere and stratosphere, around AD LEO the impact on stratospheric  $\text{O}_3$  is much fiercer, while in the troposphere the enhanced smog  $\text{O}_3$  from NOX (see Fig.

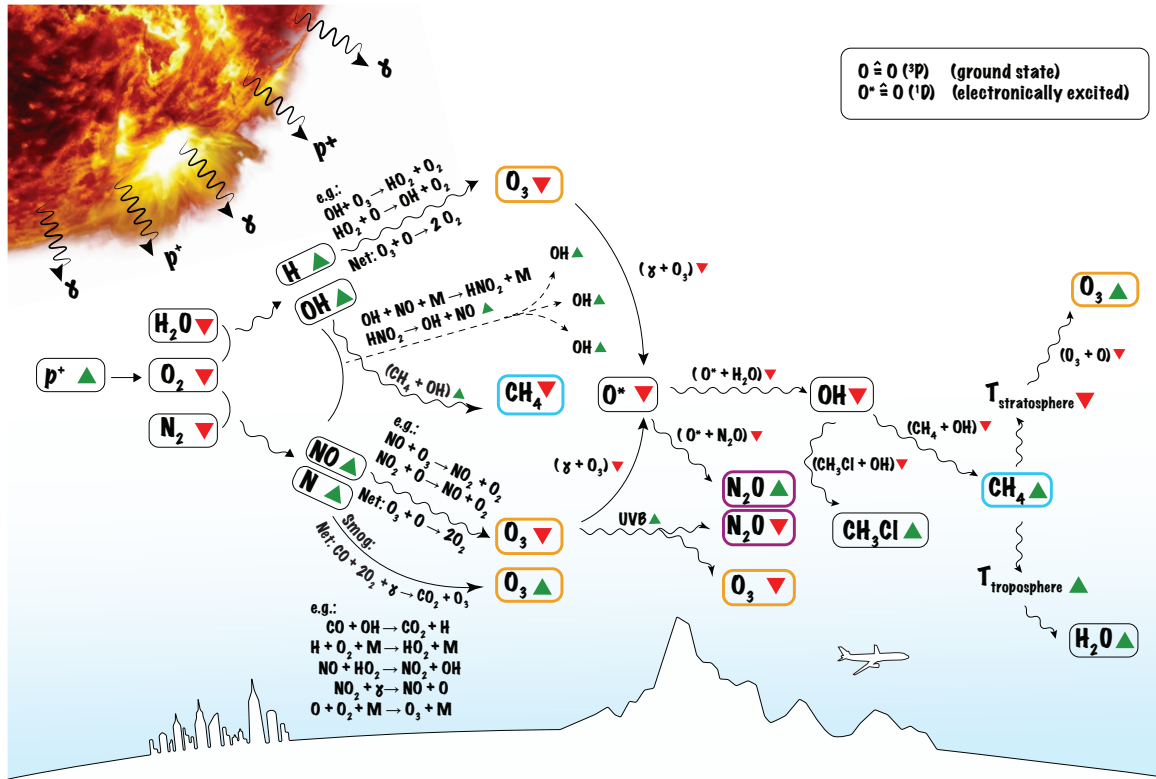


**Figure 9.** Schematic diagram showing the biosignature response (simplified) to cosmic rays ( $p^+$ ) and photons ( $\gamma$ ) from the star (upper left corner): Influx of  $p^+$  directly decreases (red downward arrows) the abundance of  $H_2O$ ,  $O_2$ , and  $N_2$ , by producing (green upward arrows)  $H$ ,  $OH$ ,  $NO$ , and  $N$ . Subsequently the abundance of other molecules also decreases (red arrows) and some increase (green arrows) via several paths and reactions (black). There are several different possible reasons for an e.g.  $O_3$  or  $CH_4$  increase or decrease, and depending on the host star radiation and  $p^+$  activity, some paths are more prominent than others, leading to different abundances. Vertical positions in the diagram provide an indication, where these processes dominate in the atmosphere. Reactions including  $\gamma + M$  are three-body reactions, while  $\gamma + \gamma$  denotes photolysis.  $O$  is the ground state atomic oxygen  $O(^3P)$ , and  $O^*$  its excited state  $O(^1D)$ .

9 for smog  $O_3$ ) together with much lower stellar UVB input i.e. less tropospheric  $O_3$  destruction by photolysis, leads to enhanced tropospheric  $O_3$  abundances. This behavior was confirmed by a detailed analysis of reaction rates of sources and sinks and related pathways. For a theoretically flaring Sun lower stratospheric  $O_3$  abundances yield higher UVB radiation in the troposphere i.e. higher tropospheric  $O_3$  photolysis rates, limiting the smog  $O_3$  build-up. For AD LEO the much lower UVB radiation cannot impact tropospheric smog  $O_3$  build up efficiently. In the high flaring cases of each host star however, our analysis shows that tropospheric  $O_3$  undergoes a transition from a smog-dominated build up to a so-called titration limited regime, where the single reaction  $NO + O_3 \rightarrow NO_2 + O_2$  dominates atmospheric  $O_3$  destruction i.e. efficiently limits  $O_3$  build up. The main sink for nitrous oxide ( $N_2O$ ) is photolysis, which is generally much slower than  $O_3$  photolysis. Despite decreased  $O_3$  for increasing flare energies (Fig. 3 and 4), hence increased UVB,  $N_2O$  values nevertheless appear to 'saturate'. We can further see this in the

UVB profiles in Fig. 6: Where stratospheric  $O_3$  is significantly reduced, UVB absorption in the stratosphere is negligible. The dependence on  $O_3$  is clearly visible in the AD LEO cases between 18-20 km where  $O_3$  shows a strong decrease with height. Only the increase in atmospheric density in the troposphere leads to a significant UVB absorption where  $O_3$  abundances are low.  $N_2O$  is never significantly destroyed by UVB in our study, even where  $O_3$  is least abundant across all our model runs.  $N_2O$  photolysis is already slower in the stratosphere than  $O_3$  photolysis, additionally eddy diffusion might redistribute  $N_2O$  faster than it is photolytically destroyed by UVB and the  $N_2O$  reaction with  $O(^1D)$  becomes  $O(^1D)$  starved hence significantly reduced where  $O_3$  abundance is lower. Such effects together may explain the  $N_2O$  behavior over a wide variety of flaring conditions. See Fig. 9 for an overview.

Due to the direct increase of  $OH$  (an important  $CH_4$  sink), one would also expect a steady reduction of  $CH_4$  with increasing flare intensity (see Fig. 3). For AD LEO cases this holds, but for high flaring Sun cases we see

a turning point, above which  $\text{CH}_4$  becomes more abundant again. This is a result of decreased OH production. In the troposphere and up to the mid stratosphere, OH is the main sink of  $\text{CH}_4$ . Above that, direct reaction with chlorine becomes the dominant contribution, at least for stellar flaring cases. This effect contributes only weakly to the total column amount however, because of the low number density. In the troposphere, where most of the methane lies, OH is produced by three main sources, the reaction of  $\text{O}(^1\text{D})$  with  $\text{H}_2\text{O}$ , NO reacting with  $\text{HO}_2$ , and the lesser studied photolysis of  $\text{HNO}_2$  (see Grenfell et al. (1995)) which becomes dominant in the lower stratosphere (this requires future work).  $\text{O}(^1\text{D})$  itself is formed almost entirely from  $\text{O}_3$  photolysis. With higher flaring and hence reduced ozone levels, there is a tipping-point, where less  $\text{O}(^1\text{D})$  produced from  $\text{O}_3$  leads to a reduction in OH. The same also happens in AD LEO runs, but at higher flaring strengths of around 200 times enhanced SPE89 SEP fluxes, due to increased levels of smog  $\text{O}_3$  and lower UVB radiation coming from AD LEO resulting in lower OH production i.e.  $\text{CH}_4$  destruction. Chloromethane, in all cases, follows the methane trends, only with smaller molecular abundances.

While the effect of varying  $f_{\text{NOx}}$  and  $f_{\text{HOx}}$  is rather weak for the Earth around Sun case, even for an artificially high flaring Sun the effect of varying these parameters for the AD LEO cases becomes very important. The lower row of Fig. 6 for a virtual Earth around AD LEO at a distance of 0.161 AU i.e.  $0.9 \text{ TSI}_{\oplus}$  shows in the high flaring SPE89x50 case that especially varying  $f_{\text{HOx}}$  can result in temperature differences throughout most of the stratosphere of around 40 K. Interestingly enough, the parameter combination of  $f_{\text{NOx}} = 2.0$  and  $f_{\text{HOx}} = 0.0$  around a high flaring AD LEO leads to a temperature profile similar to a quiescent AD LEO while stratospheric ozone abundance in this case is significantly lower (up to four orders of magnitude) than in the quiescent AD LEO cases.  $\text{O}_3$  is known to drive the stratospheric temperature inversion in Earth's atmosphere, but we would like to note here that for low stratospheric  $\text{O}_3$  abundances caused by stellar flaring i.e. reduced or complete lack of temperature inversion, other molecules such as  $\text{CH}_4$  and  $\text{H}_2\text{O}$  determine stratospheric temperatures as already discussed by e.g. Segura et al. (2005); Rauer et al. (2011); Tabataba-Vakili et al. (2016). We see the main contribution to stratospheric heating in our model from absorption of incoming stellar photons in the near infrared range between 1-2  $\mu\text{m}$ . As indicated in the transmission spectra in Fig. 7  $\text{H}_2\text{O}$  and  $\text{CH}_4$  bands have overlapping contributions and are therefore hard to distinguish. However, in contrast to

the studies mentioned above, in our study of  $f_{\text{NOx}}$  and  $f_{\text{HOx}}$  (see Fig. 8) we see a stronger correlation between temperatures and stratospheric  $\text{H}_2\text{O}$  profiles and a weakened role of  $\text{CH}_4$ .

In the modeled transit spectra in Fig. 7 we clearly show the effect of reduced ozone, methane, and water for high flaring scenarios when compared to the GCR reference case. All water and methane absorption features are reduced for the flaring case with  $f_{\text{HOx}}=0.0$ , and even more suppressed for the  $f_{\text{HOx}}=2.0$  case (light blue). Since NOx and HOx from HEPs can form  $\text{HNO}_3$  via the reaction  $\text{NO}_2+\text{OH}+\text{M}\rightarrow\text{HNO}_3+\text{M}$  this leads to the absorption features seen in Fig. 7. We confirm the  $\text{HNO}_3$  absorption around 11 microns to be an indicator for an  $\text{N}_2\text{-O}_2$  atmosphere exposed to a high flaring stellar environment, as proposed by Tabataba-Vakili et al. (2016). The second absorption feature of nitric acid around 17 microns is only visible for the case of high HOx production from cosmic ray induced ion pairs. Hence, the measurement of this absorption band may be a hint for these values of HOx production per ion pair. Rauer et al. (2011) and Hedelt et al. (2013) already analyzed the telescope time needed with a configuration based on JWST to identify various spectral features. With SNRs derived after Hedelt et al. (2013) we estimate that  $\sim 35$  transits of a theoretical planet around AD LEO (distance to observer 4.9 pc) would be needed to identify the 11 micron  $\text{HNO}_3$  band with a spectral resolution  $R=100$ . The second  $\text{HNO}_3$  feature around 17 microns might require already a few hundred transits compared to an estimated 3-4 transits with NIRSpc (in the  $R=100$  mode) onboard JWST for the 4.2 micron  $\text{CO}_2$  band. The third  $\text{HNO}_3$  absorption feature around 21 microns might be hard to detect at all, as it already lies in the far infrared where the  $\text{H}_2\text{O}$  continuum dominates.

## 5. CONCLUSIONS

We have performed atmospheric simulations of virtual Earth-like planets around the flaring M-star AD LEO with our cloud-free 1D climate-chemistry model and have compared the influence of flaring strength with the uncertainty ranges of chemical NOx-HOx production efficiencies.

New chemical insights found in this work are:

- **NOx-HOx:** The chemical production efficiencies  $f_{\text{NOx}}$  and  $f_{\text{HOx}}$  can significantly influence biosignature chemistry and abundances in our model, as well as stratospheric temperatures, and are therefore potentially important for Earth-like planets around M-dwarf stars like AD LEO. In the Earth's

atmosphere, on the other, the influx of SEPs has a much stronger effect than  $f_{\text{NOX}}$  and  $f_{\text{HOX}}$ , which makes the empirical determination of the latter challenging.

- **HNO<sub>3</sub>**: Spectroscopic transit measurements of exoplanets may be able to help constrain their stellar environments by looking at e.g. HNO<sub>3</sub> features above 10 microns together with infrared O<sub>3</sub>, H<sub>2</sub>O and CH<sub>4</sub> absorption bands. Especially the measurement of the HNO<sub>3</sub> features at 17 and 21 microns would hint towards high  $f_{\text{HOX}}$  production.
- **Cl**: We introduce and discuss a change of the major CH<sub>4</sub> sink in the stratosphere from OH (lower stratosphere) to Cl (upper stratosphere). This may also become important for worlds with e.g. high volcanic chlorine emissions.
- **O<sub>3</sub>**: We show that on Earth the UVB radiation from the Sun (G-star) is sufficient to limit global tropospheric smog O<sub>3</sub> abundances even in hypothetical high flaring Sun scenarios, while we confirm lower atmospheric build-up of O<sub>3</sub> for Earth-like planets around active M-stars like AD LEO, as has been modeled in multiple studies e.g. [Segura et al. \(2005\)](#); [Grenfell et al. \(2012\)](#); [Tabataba-Vakili et al. \(2016\)](#).
- **N<sub>2</sub>O**: Atmospheric N<sub>2</sub>O abundance runs into 'saturation' for flaring cases regardless of stellar spectrum, flaring strengths, or stratospheric O<sub>3</sub> levels. N<sub>2</sub>O reactions e.g. with O(<sup>1</sup>D) in addition to dif-

fusion processes within the atmosphere counteract the O<sub>3</sub> - UV - N<sub>2</sub>O coupling (See Fig. 9). Hence, destruction of N<sub>2</sub>O by cosmic rays is ineffective in our model.

Additionally, in our model OH is the major sink for CH<sub>4</sub> in the lower to mid atmosphere and is directly produced by SEPs, but we find that around high flaring solar-like stars atmospheric O<sub>3</sub> abundances can significantly drop, which itself is a major source of tropospheric OH production (see Fig. 9). This lack of OH from O<sub>3</sub> can outweigh OH production from SEPs, subsequently causing unexpectedly high CH<sub>4</sub> abundances (see figures 3 and 9). Furthermore, in absence of other sources HNO<sub>2</sub> can become the main OH source throughout our whole model atmosphere for high flaring host star cases. Further work on this is needed to see for which range of planetary atmospheres HNO<sub>2</sub> may become important. We would like to emphasize once more that NOX and HOX produced by cosmic rays can become important when studying Earth-like atmospheres around active M-stars.

The authors express their thanks to Christina Ciarullo for assistance with graphics.

MS acknowledges support from DFG project RA 714/9-1.

MG acknowledges support from DFG project GO 2610/1-1.

FS acknowledges support from DFG project SCHR 1125/3-1.

*Software*: GARLIC ([Schreier et al. 2014](#); [Schreier et al. 2018a,b](#)), HITRAN2012 ([Rothman et al. 2013](#))

## REFERENCES

- Airapetian, V., Glocer, A., Gronoff, G., Hébrard, E., & Danchi, W. 2016, *Nature Geoscience*, 9, 452
- Atri, D. 2017, *Monthly Notices of the Royal Astronomical Society: Letters*, 465, L34, doi: [10.1093/mnrasl/slw199](https://doi.org/10.1093/mnrasl/slw199)
- Candelaresi, S., Hillier, A., Maehara, H., Brandenburg, A., & Shibata, K. 2014, *ApJ*, 792, 67, doi: [10.1088/0004-637X/792/1/67](https://doi.org/10.1088/0004-637X/792/1/67)
- Cess, R. D. 1976, *Journal of Atmospheric Sciences*, 33, 1831, doi: [10.1175/1520-0469\(1976\)033<1831:CCAAOA>2.0.CO;2](https://doi.org/10.1175/1520-0469(1976)033<1831:CCAAOA>2.0.CO;2)
- Clough, S., Kneizys, F., & Davies, R. 1989, *Atmospheric Research*, 23, 229, doi: [https://doi.org/10.1016/0169-8095\(89\)90020-3](https://doi.org/10.1016/0169-8095(89)90020-3)
- Crutzen, P. J. 1970, *Quarterly Journal of the Royal Meteorological Society*, 96, 320, doi: [10.1002/qj.49709640815](https://doi.org/10.1002/qj.49709640815)
- Fichtner, H., Heber, B., Herbst, K., Kopp, A., & Scherer, K. 2013, in *Climate and Weather of the Sun-Earth System (CAWSES)* (Springer), 55–78
- Fujii, Y., Del Genio, A. D., & Amundsen, D. S. 2017, *ApJ*, 848, 100, doi: [10.3847/1538-4357/aa8955](https://doi.org/10.3847/1538-4357/aa8955)
- Gardner, J. P., Mather, J. C., Clampin, M., et al. 2006, *SSRv*, 123, 485, doi: [10.1007/s11214-006-8315-7](https://doi.org/10.1007/s11214-006-8315-7)
- Godolt, M., Grenfell, J. L., Kitzmann, D., et al. 2016, *A&A*, 592, A36, doi: [10.1051/0004-6361/201628413](https://doi.org/10.1051/0004-6361/201628413)
- Godolt, M., Grenfell, J. L., Hamann-Reinus, A., et al. 2015, *Planet. Space Sci.*, 111, 62, doi: [10.1016/j.pss.2015.03.010](https://doi.org/10.1016/j.pss.2015.03.010)
- Grenfell, B. T., Bolker, B. M., & Kleczkowski, A. 1995, *Proceedings of the Royal Society of London Series B*, 259, 97
- Grenfell, J. L., Griebmeier, J.-M., von Paris, P., et al. 2012, *Astrobiology*, 12, 1109, doi: [10.1089/ast.2011.0682](https://doi.org/10.1089/ast.2011.0682)

- Grieffmeier, J.-M., Stadelmann, A., Grenfell, J. L., Lammer, H., & Motschmann, U. 2009, *Icarus*, 199, 526, doi: [10.1016/j.icarus.2008.09.015](https://doi.org/10.1016/j.icarus.2008.09.015)
- Grieffmeier, J.-M., Stadelmann, A., Motschmann, U., et al. 2005, *Astrobiology*, 5, 587, doi: [10.1089/ast.2005.5.587](https://doi.org/10.1089/ast.2005.5.587)
- Grieffmeier, J.-M., Tabataba-Vakili, F., Stadelmann, A., Grenfell, J. L., & Atri, D. 2016, *A&A*, 587, A159, doi: [10.1051/0004-6361/201425452](https://doi.org/10.1051/0004-6361/201425452)
- Gueymard, C. A. 2004, *Solar Energy*, 76, 423 , doi: <https://doi.org/10.1016/j.solener.2003.08.039>
- Haagen-Smit, A. J. 1952, *Industrial & Engineering Chemistry*, 44, 1342
- Hawley, S. L., & Pettersen, B. R. 1991, *ApJ*, 378, 725, doi: [10.1086/170474](https://doi.org/10.1086/170474)
- Hedelt, P., von Paris, P., Godolt, M., et al. 2013, *A&A*, 553, doi: [10.1051/0004-6361/201117723](https://doi.org/10.1051/0004-6361/201117723)
- Kasper, M., Beuzit, J.-L., Verinaud, C., et al. 2010, in *Ground-based and Airborne Instrumentation for Astronomy III*, Vol. 7735, International Society for Optics and Photonics, 77352E
- Kasting, J. F., & Ackerman, T. P. 1986, *Science*, 234, 1383, doi: [10.1126/science.234.4782.1383](https://doi.org/10.1126/science.234.4782.1383)
- Kasting, J. F., Whitmire, D. P., & Reynolds, R. T. 1993, *Icarus*, 101, 108, doi: [10.1006/icar.1993.1010](https://doi.org/10.1006/icar.1993.1010)
- Kopparapu, R. k., Wolf, E. T., Haqq-Misra, J., et al. 2016, *ApJ*, 819, 84, doi: [10.3847/0004-637X/819/1/84](https://doi.org/10.3847/0004-637X/819/1/84)
- Kopparapu, R. K., Ramirez, R., Kasting, J. F., et al. 2013, *ApJ*, 765, 131, doi: [10.1088/0004-637X/765/2/131](https://doi.org/10.1088/0004-637X/765/2/131)
- Leconte, J., Forget, F., Charnay, B., Wordsworth, R., & Pottier, A. 2013, *Nature*, 504, 268, doi: [10.1038/nature12827](https://doi.org/10.1038/nature12827)
- Luger, R., & Barnes, R. 2015, *Astrobiology*, 15, 119
- Maehara, H., Shibayama, T., Notsu, S., et al. 2012, *Nature*, 485, 478, doi: [10.1038/nature11063](https://doi.org/10.1038/nature11063)
- Manabe, S., & Wetherald, R. T. 1967, *Journal of Atmospheric Sciences*, 24, 241, doi: [10.1175/1520-0469\(1967\)024<0241:TEOTAW>2.0.CO;2](https://doi.org/10.1175/1520-0469(1967)024<0241:TEOTAW>2.0.CO;2)
- Marcq, E., Belyaev, D., Montmessin, F., et al. 2011, *Icarus*, 211, 58 , doi: <https://doi.org/10.1016/j.icarus.2010.08.021>
- Melsheimer, C., Verdes, C., Buehler, S., et al. 2005, *Radio Science*, 40
- Murphy, W. F. 1977, *The Journal of Chemical Physics*, 67, 5877, doi: [10.1063/1.434794](https://doi.org/10.1063/1.434794)
- Popp, M., Schmidt, H., & Marotzke, J. 2015, *Journal of Atmospheric Sciences*, 72, 452, doi: [10.1175/JAS-D-13-047.1](https://doi.org/10.1175/JAS-D-13-047.1)
- Porter, H. S., Jackman, C. H., & Green, A. E. S. 1976, *JChPh*, 65, 154, doi: [10.1063/1.432812](https://doi.org/10.1063/1.432812)
- Ramirez, R. M., & Kaltenegger, L. 2014, *The Astrophysical Journal Letters*, 797, L25
- Rauer, H., Gebauer, S., Paris, P. V., et al. 2011, *A&A*, 529, A8, doi: [10.1051/0004-6361/201014368](https://doi.org/10.1051/0004-6361/201014368)
- Rothman, L. S., Gordon, I. E., Babikov, Y., et al. 2013, *JQSRT*, 130, 4, doi: [10.1016/j.jqsrt.2013.07.002](https://doi.org/10.1016/j.jqsrt.2013.07.002)
- Rugheimer, S., Kaltenegger, L., Segura, A., Linsky, J., & Mohanty, S. 2015a, *ApJ*, 809, 57, doi: [10.1088/0004-637X/809/1/57](https://doi.org/10.1088/0004-637X/809/1/57)
- Rugheimer, S., Segura, A., Kaltenegger, L., & Sasselov, D. 2015b, *ApJ*, 806, 137, doi: [10.1088/0004-637X/806/1/137](https://doi.org/10.1088/0004-637X/806/1/137)
- Rusch, D., Grard, J.-C., Solomon, S., Crutzen, P., & Reid, G. 1981, *Planet. Space Sci.*, 29, 767 , doi: [http://dx.doi.org/10.1016/0032-0633\(81\)90048-9](http://dx.doi.org/10.1016/0032-0633(81)90048-9)
- Scalo, J., Kaltenegger, L., Segura, A. G., et al. 2007, *Astrobiology*, 7, 85, doi: [10.1089/ast.2006.0125](https://doi.org/10.1089/ast.2006.0125)
- Schreier, F., Gimeno García, S., Hedelt, P., et al. 2014, *JQSRT*, 137, 29, doi: [10.1016/j.jqsrt.2013.11.018](https://doi.org/10.1016/j.jqsrt.2013.11.018)
- Schreier, F., Milz, M., Buehler, S., & von Clarmann, T. 2018a, *J. Quant. Spectrosc. & Radiat. Transfer*, 211, 64, doi: [10.1016/j.jqsrt.2018.02.032](https://doi.org/10.1016/j.jqsrt.2018.02.032)
- Schreier, F., Städt, S., Hedelt, P., & Godolt, M. 2018b, *Molec. Astrophysics*, 11, 1, doi: [10.1016/j.molap.2018.02.001](https://doi.org/10.1016/j.molap.2018.02.001)
- Segura, A., Kasting, J. F., Meadows, V., et al. 2005, *Astrobiology*, 5, 706, doi: [10.1089/ast.2005.5.706](https://doi.org/10.1089/ast.2005.5.706)
- Segura, A., Krellove, K., Kasting, J. F., et al. 2003, *Astrobiology*, 3, 689, doi: [10.1089/153110703322736024](https://doi.org/10.1089/153110703322736024)
- Segura, A., Walkowicz, L. M., Meadows, V., Kasting, J., & Hawley, S. 2010, *Astrobiology*, 10, 751, doi: [10.1089/ast.2009.0376](https://doi.org/10.1089/ast.2009.0376)
- Selsis, F. 2000, in *ESA Special Publication*, Vol. 451, *Darwin and Astronomy : the Infrared Space Interferometer*, ed. B. Schürmann, 133
- Shibayama, T., Maehara, H., Notsu, S., et al. 2013, *ApJS*, 209, 5, doi: [10.1088/0067-0049/209/1/5](https://doi.org/10.1088/0067-0049/209/1/5)
- Shields, A. L., Ballard, S., & Johnson, J. A. 2016, *PhR*, 663, 1, doi: [10.1016/j.physrep.2016.10.003](https://doi.org/10.1016/j.physrep.2016.10.003)
- Shields, A. L., Meadows, V. S., Bitz, C. M., et al. 2013, *Astrobiology*, 13, 715, doi: [10.1089/ast.2012.0961](https://doi.org/10.1089/ast.2012.0961)
- Sinnhuber, M., Nieder, H., & Wieters, N. 2012, *Surveys in Geophysics*, 33, 1281, doi: [10.1007/s10712-012-9201-3](https://doi.org/10.1007/s10712-012-9201-3)
- Smart, D. F., & Shea, M. A. 2002, *Advances in Space Research*, 30, 1033, doi: [10.1016/S0273-1177\(02\)00497-0](https://doi.org/10.1016/S0273-1177(02)00497-0)
- Sneep, M., & Ubachs, W. 2005, *Journal of Quantitative Spectroscopy and Radiative Transfer*, 92, 293
- Solomon, S., Rusch, D., Grard, J., Reid, G., & Crutzen, P. 1981, *Planet. Space Sci.*, 29, 885 , doi: [http://dx.doi.org/10.1016/0032-0633\(81\)90078-7](http://dx.doi.org/10.1016/0032-0633(81)90078-7)

Tabataba-Vakili, F., Grenfell, J. L., Griebmeier, J.-M., & Rauer, H. 2016, *A&A*, 585, A96, doi: [10.1051/0004-6361/201425602](https://doi.org/10.1051/0004-6361/201425602)

Tian, F., & Ida, S. 2015, *Nature Geoscience*, 8, 177

Verronen, P. T., & Lehmann, R. 2013, *Annales Geophysicae*, 31, 909, doi: [10.5194/angeo-31-909-2013](https://doi.org/10.5194/angeo-31-909-2013)

von Clarmann, T., Hopfner, M., Funke, B., et al. 2003, *JQSRT*, 78, 381, doi: [10.1016/S0022-4073\(02\)00262-5](https://doi.org/10.1016/S0022-4073(02)00262-5)

Yang, J., Boué, G., Fabrycky, D. C., & Abbot, D. S. 2014, *ApJL*, 787, L2, doi: [10.1088/2041-8205/787/1/L2](https://doi.org/10.1088/2041-8205/787/1/L2)